iMRI 2023;27(4);182-195
https://doi.org/10.13104/imri.2023.0029
eISSN 2384-1109

Review Article

Received: October 17, 2023
Revised: November 22, 2023
Accepted: November 27, 2023

Correspondence
Bio Joo, MD, PhD
Department of Radiology,
Gangnam Severance Hospital,
Yonsei University
College of Medicine,
211 Eonju-ro, Gangnam-gu,
Seoul 06273, Korea.
E-mail: yonnebio@yuhs.ac

Magnetic Resonance Elastography for Clinicians and Researchers Unfamiliar With the Field

Seungtae Lee, Bio Joo, Mina Park, Sung Jun Ahn, and Sang Hyun Suh

Department of Radiology, Gangnam Severance Hospital, Yonsei University College of Medicine, Seoul, Korea

Magnetic resonance elastography (MRE) is an emerging magnetic resonance imaging (MRI) technique capable of quantitatively evaluating the biomechanical properties of tissue. MRE has been widely used in the evaluation of chronic parenchymal liver diseases. However, numerous studies have suggested its applicability in evaluating other organs. The MRE data acquisition process consists of three main steps: 1) generation of mechanical waves in soft tissues; 2) adoption of a modified phase-contrast MRI sequence to capture tissue displacements produced by the propagation of applied waves; and 3) application of an inversion algorithm to transform the wave image into maps of viscoelastic properties. As efforts are made to standardize MRE terminology and protocols, more extensive clinical investigations using MRE are expected in the future.

Keywords: Magnetic resonance elastography; Viscoelastic properties; Shear stiffness; Stiffness

INTRODUCTION

Magnetic resonance elastography (MRE) is an emerging magnetic resonance imaging (MRI) technique capable of quantitatively evaluating tissue biomechanical properties, and was first documented by Muthupillai et al. in 1995 [1]. This method provides a form of quantitative, noninvasive palpation that has been used as an effective clinical diagnostic technique for centuries [2].

MRE has been widely used to evaluate chronic parenchymal liver disease, and is regarded as an excellent method for assessing liver fibrosis [3]. In addition, numerous studies have suggested its applicability for evaluating other organs, such as the brain [4,5].

However, the wide variety of acquisition and processing methods, combined with the results presented in different metrics, addressing MRE studies challenging [2]. In this general review of MRE, emphasis is placed on elucidating the fundamental principles underpinning MRE, rather than exploring the specific results of studies related to individual organs or diseases, catering to readers with limited prior knowledge of MRE. The following topics are discussed: 1) mechanical properties of soft tissues; 2) methodology of MRE; 3) clinical applications of MRE in the liver, brain, and other organs; and 4) limitations, recent advancements, and future perspectives of the technique.

Mechanical Properties of Soft Tissue

Waves propagate faster and have longer wavelengths in stiffer materials. In soft tissues, longitudinal waves travel at high speeds (approximately 1540 m/s) with long wavelengths, and their velocities remain relatively consistent across different tissues. However, shear (transverse) waves within the frequency range of interest for MRE propagate at speeds between 1–5 m/s with variability in speed among different tissues. Therefore, MRE utilizes shear wave propagation within the target tissues to delineate the relationship between shear strain and shear stress, which is termed the 'shear modulus' (Fig. 1).

In addition to shear modulus, elasticity and viscosity are two fundamental concepts in MRE. Elasticity refers to the ability of an object or material to return to its initial size or shape once deforming forces are removed. Conversely, viscosity is a material property that relates the stresses in a material to the rate of change in deformation, and involves the absorption of mechanical energy during deformation [2,6]. Under the assumption that materials are isotropic and purely elastic, the shear modulus μ is calculated as follows:

$$\mu = \rho v_s^2 \text{ and } v_s = \lambda f \quad \text{Eq. (1)}$$

where ρ is the soft tissue density, which is assumed to be 1000 kg/m^3 [7], v_s represents the speed of the shear wave (m/s), λ denotes the wavelength of the shear wave (m), and f is the frequency of the shear wave (Hz) [8]. Hence, if the local wavelength λ or velocity v_s of propagating shear waves is measured, the shear modulus can be calculated.

However, most soft tissues simultaneously display both elastic and viscous characteristics, behaving slightly like solids and fluids, making them 'viscoelastic.' For such materials, the term 'complex shear modulus (G^*)' is commonly introduced in MRE:

$$G^* = G' + iG''. \quad \text{Eq. (2)}$$

It comprises a storage modulus (G'), the real part of the complex shear modulus, which represents elasticity, and a loss modulus (G''), the imaginary part, which represents viscosity. In addition, the damping ratio (ζ), defined as $G''/(2G')$, is another commonly used parameter to quantify the magnitude of the loss modulus relative to that of the storage modulus.

These can be represented in polar coordinates using the magnitude $|G^*|$ and phase angle φ (also called as loss tangent) of the complex shear modulus G^* (Fig. 2):

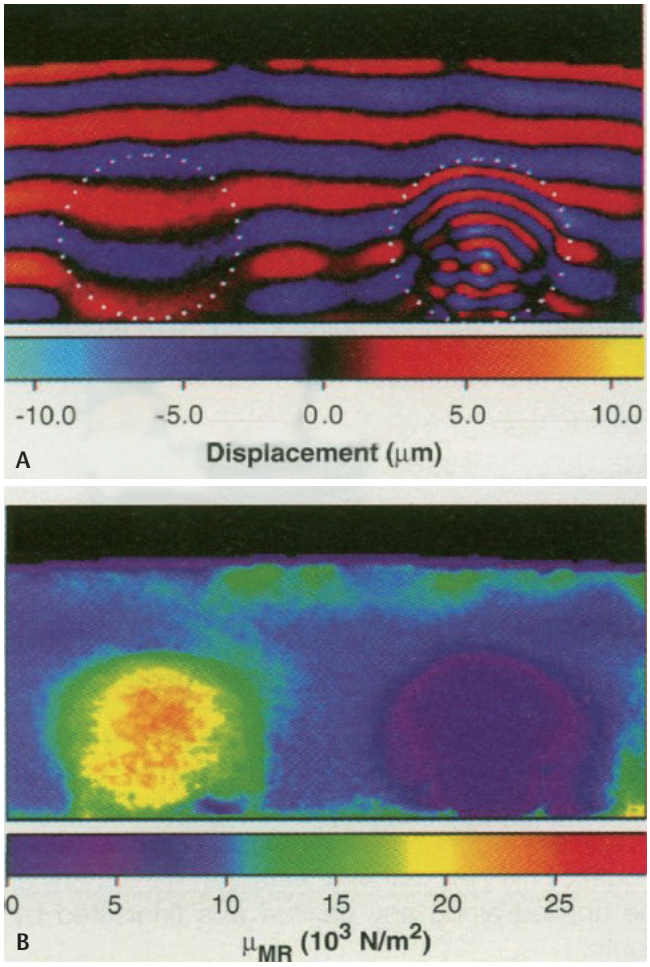

Fig. 1. Figures from the first MRE publication demonstrating the propagation of shear waves in a gel phantom. A: Wave image illustrating different patterns of shear wave propagation within two cylinders embedded in a tissue-simulating gel phantom. The left cylinder, which was stiffer, exhibited a longer wavelength than the surrounding gel, whereas the softer cylinder on the right showed a shorter wavelength. B: Quantitative map of the shear modulus computed from the local wavelength of the wave image. Adapted with permission from Muthupillai et al. [1], Science 1995;269:1854-1857. MRE, magnetic resonance elastography; MR, magnetic resonance.

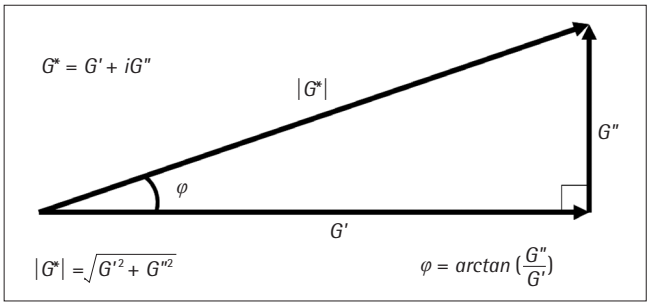

Fig. 2. Vector diagram of the complex shear modulus G^*. G' denotes the storage modulus and indicates a material's capacity to store energy. G'' denotes the loss modulus, related to the amount of energy loss via viscous processes. The complex shear modulus G^* is represented as $G^* = G' + iG''$. These can be represented in polar coordinates using the magnitude $|G^*|$ and phase angle φ.

$$|G^*| = \sqrt{G'^2 + G''^2} \text{ and } \varphi = arctan\left(\frac{G''}{G'}\right). \quad \text{Eq. (3)}$$

In this context of viscoelastic materials, the shear modulus μ can vary with frequency. The data from MRE can be described using the term 'shear stiffness (Gs or μ)', which indicates the 'effective' shear modulus at a particular frequency, through the following equation with its relationship to the complex shear modulus, under the assumption that the density ρ equals 1 g/cm^{-3} [8,9]:

$$G_s = \rho v_s^2 = \frac{2|G^*|^2}{G' + |G^*|}. \quad \text{Eq. (4)}$$

In purely elastic materials, there is no phase lag or energy dissipation; thus, the loss modulus G'' becomes zero. In contrast, a greater phase angle φ or damping ratio ζ indicates more viscous behavior in the tissue. The magnitude $|G^*|$ encompasses both elasticity and viscosity, and has been reported to closely approximate the information obtained by manual palpation [5]. Conversely, the phase angle φ has been reported to reflect the complexity of the tissue architecture [10]. Technically, the phase angle φ denotes the relationship between elasticity and viscosity. However, it is frequently reported as an indicator of tissue viscosity because the loss moduli are an order of magnitude smaller than the storage moduli [5].

However, the aforementioned parameters depend on the applied frequency, making them specific to certain experimental conditions. Because the majority of soft tissues show distinct wave speeds at different frequencies, using multifrequency MRE and reporting frequency-independent material parameters may be preferred for measuring their viscoelastic properties [11]. This is achieved by fitting the MRE data acquired across different vibration frequencies to a specific mathematical representation known as the rheological model [12-15]. There are several rheological models, some of which can describe the viscoelastic behavior of materials under dynamic (oscillating) stresses, as is the case in MRE [6]. Among these, the spring-pot model, in which the tissue is characterized by a hierarchical arrangement of elastic 'springs' and viscous 'dashpots,' has been reported to represent the biological tissue behavior better than other models within the MRE frequency range [6,13]. In the spring-pot model, the complex shear moduli data over different frequencies were fitted using the following equation:

$$G^* = k\,(i \cdot 2\pi \cdot f)^{\alpha} \text{ and } k = \mu^{(1-\alpha)}\eta^{\alpha}. \quad \text{Eq. (5)}$$

The variable k can be transferred to a spring-pot parameter μ by assuming the viscosity η at an empirical value, for example, a value of 3.7 Pa · s for brain tissue and 7.3 Pa · s for liver [12,15]. Finally, two frequency-independent parameters, spring-pot parameter μ and power-law coefficient α are obtained. The spring-pot parameter μ integrates both elastic and viscous information, illustrating the tissue's solid-fluid characteristics as an indicator of the adhesion and connectivity of soft tissue [13]. However, the power-law coefficient α is known as the geometry parameter and reflects material complexity [14,16]. A purely elastic solid has $\alpha = 0$, while a viscous fluid without energy restoration is characterized by $\alpha = 1$. Fundamentally, the power-law coefficient α is not directly comparable to the phase angle φ of the complex shear modulus, which is frequency-dependent. However, for complex and irregular materials like biological tissues, φ becomes less sensitive to frequency. Consequently, $\varphi = \alpha \times \pi/2$ could be applicable [17]. Therefore, viscosity may be parameterized by the power-law coefficient α in MRE [2].

Notably, a common method to describe the mechanical properties of soft tissue is to refer to its 'stiffness.' However, from a biomechanical perspective, the term 'stiffness' is not precise; there are several different definitions of stiffness, such as structural stiffness, bending stiffness, and torsional stiffness [18]. Therefore, the MRE Guidelines Committee recently recommended using the term 'stiffness' solely for qualitative statements or, if used otherwise, to specify the definition of stiffness being referred to [2]. Nonetheless, numerous studies have used the term 'stiffness' in various contexts. Similarly, the term 'shear stiffness' has been defined in various ways, with some referring to the magnitude $|G^*|$ and others to that derived from the wave speed estimation [19,20]. Therefore, care should be taken when interpreting and comparing those results.

The various terminology and metrics employed by different research groups make it challenging to understand and interpret MRE study results. Although these metrics may not be directly comparable, they can be broadly categorized into two groups based on their relative sensitivity or relevance to specific mechanical properties: stiffness- and viscosity-related metrics (Table 1).

Table 1. Metrics in MRE grouped by their relative sensitivity or relevance to specific mechanical properties

Metrics more related to stiffness	Metrics more related to viscosity
Storage modulus (G')	Loss modulus (G'')
Magnitude of the complex shear modulus ($\|G^*\|$)	Phase angle of the complex shear modulus (φ)
Shear stiffness (ρv_s^2)	Loss tangent
Shear wave speed	Damping ratio (ζ)
Spring-pot parameter μ	Spring-pot parameter α

MRE, magnetic resonance elastography.

Methodology of MRE

The MRE data acquisition process consists of three main steps: 1) generation of mechanical waves in soft tissues; 2) adoption of a *modified* phase-contrast MRI sequence to capture tissue displacements produced by the propagation of applied waves; and 3) application of an inversion algorithm to transform the wave image into maps of viscoelastic properties.

Generation of Mechanical Waves in Soft Tissues

Because MRE rely on the response of soft tissues to mechanical waves, a vibration source is essential to introduce these waves into the target tissue under investigation. The typical frequency range of the waves used in MRE is 20–100 Hz [21]. Various approaches have been suggested for generating mechanical waves, including pneumatic [22-24], electromechanical [25,26], piezoelectric [27,28], and gravitational transducer systems [29-31]. Among these, pneumatic MRE driver systems are widely used in commercial MRE and are available from various MRI vendors [2]. The pneumatic system consists of a non-MRI-compatible active driver and an MRI-compatible passive driver. The active driver is located outside the scanning room and generates acoustic wave motion. The passive driver is placed over the desired organ and connected to the active driver through an air-filled plastic tube that conveys pneumatic vibrations. Passive drivers can be tailored to diverse shapes for contact optimization. For instance, a drum- or disc-shaped configuration may be employed for abdominal applications, whereas a head-pillow form can be used for brain MRE [23,24] (Figs. 3, 4). The waves generated by the MRE driver systems are converted into transverse shear waves at the internal tissue interfaces, which can be captured using a modified phase-contrast MRI sequence.

Adoption of a Modified Phase-Contrast MRI Sequence

Propagating shear waves induce cyclic motion in tissues that is typically a few microns in amplitude, which is considerably below the spatial resolution achievable with conventional MRI techniques. However, these small-scale tissue displacements can be imaged using a phase-contrast MRI technique that incorporates an oscillating motion-encoding gradient (MEG), or motion-sensitizing gradient. By switching the polarity of the

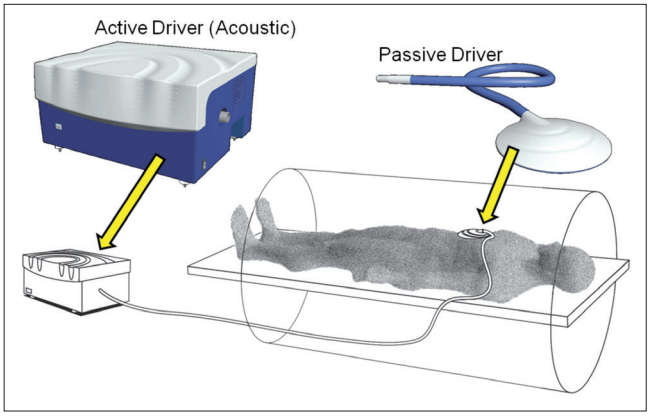

Fig. 3. Illustration of a pneumatic driver system for liver MRE. The source of mechanical waves is a device referred to as an active driver located outside of the scanner room. A flexible, air-filled plastic tubes transfers pressure waves to a non-metallic passive driver placed in contact with the body. On the surface of the passive driver, vibrations are introduced into the body to generate propagating shear waves. Adapted with permission from Venkatesh et al. [24], J Magn Reson Imaging 2013;37:544-555. MRE, magnetic resonance elastography.

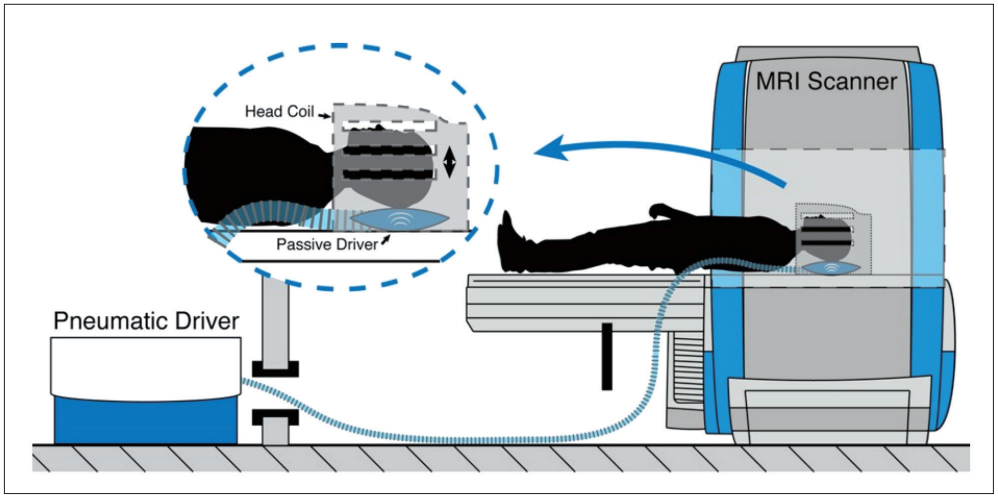

Fig. 4. Illustration of brain MRE using the pneumatic driver system with a head-pillow passive driver. A pillow-like passive driver, which receives vibrations from the active driver located in the control room, is positioned under the subject's head and introduces the vibration into the brain. Adapted with permission from Klatt et al. [137], J Magn Reson Imaging 2015;42:297-304. MRE, magnetic resonance elastography; MRI, magnetic resonance imaging.

MEG to the same frequency as the externally applied vibration, protons moving at the synchronized frequency continue to accumulate phase. The phase shifts are calculated as follows:

$$\phi(\tau) = \gamma \int_0^\tau \vec{G}_r(t) \cdot \vec{r}(t)\, dt \quad \text{Eq. (6)}$$

where γ is the gyromagnetic ratio, $\vec{G}_r(t)$ is a magnetic field gradient, τ is the period of the gradient waveform, and $\vec{r}(t)$ is the spin position. From the phase shifts calculated at a single time point, it is possible to determine the amount of tissue displacement at each voxel because the phase of the harmonically vibrating tissue is directly proportional to its displacement [1]. The synchronization between the MEG and the external vibration can be adjusted using a trigger pulse, which introduces a small delay, referred to as the phase offset. Typically, four- or eight-phase offsets are used to acquire multiphase images at different time points throughout a wave cycle (Fig. 5). After acquiring raw phase images, phase unwrapping is required (Fig. 6). Next, the removal of longitudinal waves is necessary because they may contribute to the total measured displacement field, acting as a confounding factor. High-pass filtering to remove long wavelengths or assuming the curl of the measured wave field are two common techniques for removing their contribution to the data [32-34].

MEG measures tissue movement in the direction to which it is applied. Although MRE research commonly uses two-dimensional (2D) wave propagation, recent advancements in ac-

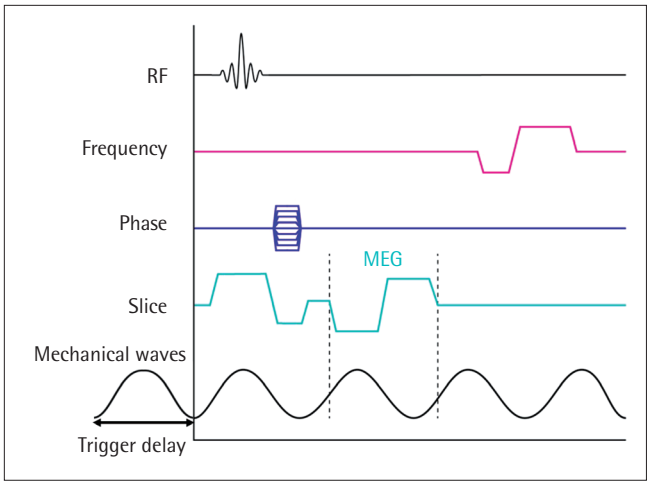

Fig. 5. MRE pulse sequence diagram. The frequency of the motion-encoding gradient is synchronized to the frequency of the mechanical waves and trigger pulse. Here, the motion-encoding gradient is implemented in the slice-select gradient. It can be sequentially applied in the x, y, and z directions. By adjusting the trigger delay, phase shifts are introduced. MRE, magnetic resonance elastography; RF, radiofrequency; MEG, motion-encoding gradient.

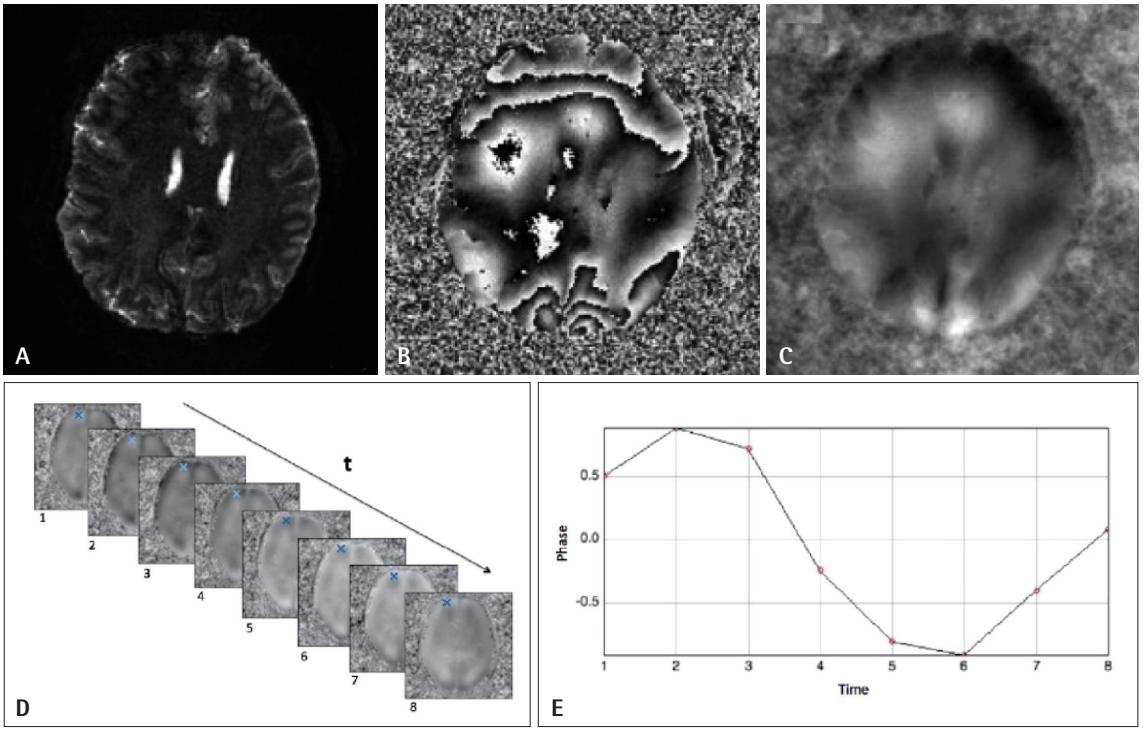

Fig. 6. Example of phase offset and phase unwrapping in brain MRE. Magnitude image (A), raw phase (wrapped) image (B), and unwrapped phase image (C) of a single slice of brain MRE are demonstrated. D: An image stack of eight phase offsets for a single brain slice is presented. The blue crosses indicate the voxel where the phase displacement is depicted in the corresponding graph (E). Adapted with permission from Hiscox et al. [5], Phys Med Biol 2016;61:R401-R437. MRE, magnetic resonance elastography.

quisition protocols have enabled MRE studies to encode full 3D wave vectors by applying MEG in all three orthogonal directions [19,35,36]. Furthermore, MEG can be incorporated into a wide range of sequences, such as gradient-recalled echo, spin-echo, balanced steady-state free precession, echo-planar imaging, and spiral sequences [4].

Application of Inversion Algorithm

The conversion of the displacement data into maps of mechanical properties, such as elastograms, can be achieved using a mathematical inversion algorithm. There are various analytical methods for calculating the shear mechanical properties based on different assumptions, each with its own advantages and drawbacks [37]. Under the assumptions of local homogeneity, isotropy, and tissue incompressibility, tissue mechanical properties are locally constant within a small local neighborhood, not direction-dependent, and incompressible because of the large water content. An algorithm called direct inversion (DI) is commonly used. The DI and its variable forms involve incorporating the measured displacements into the wave equation to directly calculate the complex shear modulus [38]. This approach is based on the assumption that the acquired wave data are sufficiently accurate to be input into the governing equations, and hence are intrinsically sensitive to data quality [37]. It provides rapid processing speed, making it suitable for a clinical radiological workflow; however, its oversimplified assumptions may compromise accuracy [2,5].

An alternative method, non-linear inversion (NLI), utilizes a finite element model (FEM) to iteratively solve the forward wave equation, minimizing the discrepancy between the FEM forward model and the observed displacement field [39]. Although this approach fundamentally provides a more accurate representation of motion physics for arbitrary materials, it is computationally intensive and highly dependent on model assumptions, such as initial stiffness values and boundary conditions [37]. Recently, several advancements beyond these methods have been introduced to enhance accuracy, reduce sensitivity to noise, and address the limitations associated with various assumptions [40-42].

Apart from the DI and NLI methods, where the resulting mechanical properties are frequency-dependent, there are additional techniques based on multi-frequency MRE that yield frequency-independent parameters. One such approach is rheological modeling. In rheological modeling, data acquired at multiple frequencies are analyzed to align with a specific rheological model, for example, Maxwell, Kelvin-Voigt, or spring-pot model, yielding frequency-independent parameters, e.g. spring-pot parameter μ and α [12,13,43].

Another alternative analysis method is the multi-frequency dual-parameter elasto-visco inversion (MDEV). MDEV employs DI analysis across multiple frequencies and integrates them into a single inversion [44]. Contrary to rheological modeling studies, MDEV assumes that tissues remain frequency-independent within a limited range of frequencies. This approach compensates for amplitude nulls and noise by averaging the displacement magnitudes in each voxel, resulting in enhanced quality and spatial resolution of mechanical property maps [26,44,45]. Notably, because parameters from MDEV, such as magnitude $|G^*|$ and phase angle φ, are derived from data across multiple frequencies but merged into allegedly frequency-independent values, they are not directly comparable to values from single frequency studies.

Another method of analysis is from the wave perspective. Within this analytical framework, the local frequency estimation (LFE) and phase gradient (PG) are typically used. These calculations only consider the local wavelength, and do not consider attenuation, which adheres to a purely elastic condition. The LFE estimates the local spatial frequency of the wave field, which is then converted to wave speed and ultimately to shear stiffness. PG algorithms simply consider the phase of the harmonic component at the driving frequency. If the motion is a simple shear wave, the gradient of this phase represents the phase shift per pixel in the direction of the wave, which can be translated into wave speed and, in turn, shear stiffness. This method yields inaccurate results when multiple waves are superimposed; thus, directional filtering is typically required to suppress reflections and interfering waves [2,8].

Clinical Applications of MRE

Liver

Currently, MRE are most actively utilized in the liver in clinical settings. MRE-based stiffness measurements have been reported to be highly consistent, demonstrating high repeatability and reproducibility, and independence from fatty change of the liver parenchyma or obesity [46-50].

In routine clinical practice, most liver MRE scans are performed using regulatory-approved commercial MRE hardware and software (Resoundant; Mayo Foundation for Medical Education and Research, Mayo Clinic, Rochester, MN, USA). This system operates on a pneumatic driver that typically uses a frequency of 60 Hz. It presents the viscoelastic parameters based on a freehand-drawn regions of interest (ROIs) covering the largest part of the liver parenchyma of the right lobe within a 95% confidence map [51].

Multiple studies have confirmed the value of MRE for noninvasive assessment of liver fibrosis [52] (Fig. 7). Currently, it is regarded as the most accurate imaging tool for the diagnosis and staging of liver fibrosis [53]. Singh et al. [54] conducted a systematic review and meta-analysis of 12 studies involving 697 patients with a less than one year interval between MRE and liver biopsy, and found that MRE had high accuracy in the di-

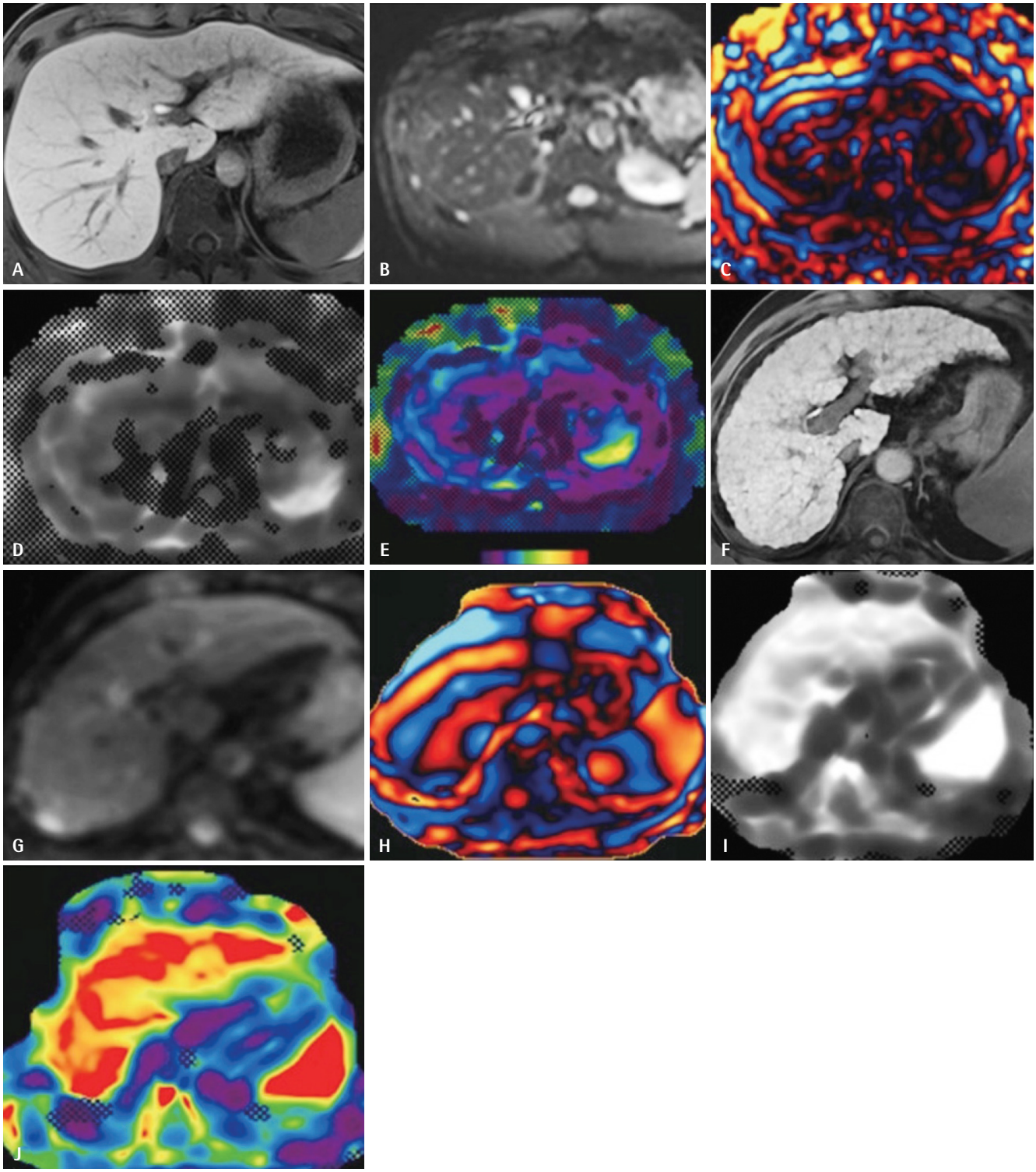

Fig. 7. Comparison of MRE findings regarding the liver stiffness. In a 29-year-old male living liver donor candidate, spin-echo MRE at 3T is depicted from (A-E), while in a 63-year-old male patient with cirrhosis, gradient echo MRE at 3T is shown from (F-J). The hepatobiliary phase images (A, F) reveal uniform contrast absorption. The magnitude (B, G) and wave (C, H) image data are then transformed into gray-scale images (D, I) and color elastograms (E, J). The wave images of the cirrhotic patient (H) display a faster wave speed compared to the healthy donor (C), consistent with increased liver stiffness observed in both gray-scale and color elastograms (I, J). Adapted from Ringe et al. [138], Korean J Radiol 2023;24:180-189, under CC BY NC license. MRE, magnetic resonance elastography.

agnosis of significant (F2) or advanced fibrosis (F3) and cirrhosis (F4), regardless of the etiology of chronic liver disease (CLD). Another meta-analysis by Su et al. [55] of 13 studies involving 989 patients reported that MRE had high diagnostic performance for the detection and staging of liver fibrosis, with a pooled area under the ROC curve of 0.95 for F ≥ 1, 0.97 for F ≥ 2, 0.97 for F ≥ 3, and 0.98 for F4.

Stiffness measurement obtained from MRE has been reported as an independent risk factor for the development of hepatocellular carcinoma in patients with CLD [56-58]. In addition, several studies have shown the role of liver MRE in the prediction of esophageal varices or decompensation along with splenic stiffness measurements [59-62].

Brain

Many studies have shown that brain MRE has the potential to provide clinically useful information by demonstrating differences in viscoelastic properties among different anatomical regions, between normal brain tissue and a range of neurological conditions, and how they change with age. However, compared to liver MRE, brain MRE is less standardized, leading to a wider range of approaches. The two most common vibration sources for brain MRE are a pneumatic driver system with a head-pillow passive driver and a head rocker unit with a rigid rod, typically utilizing a frequency range of 50–60 Hz [22,63,64]. Additionally, various research groups have adopted distinct methodologies for sequences and inversion algorithms. Therefore, direct comparisons of the reported values between brain MRE studies should be performed with caution.

Several studies have investigated the differences in viscoelastic properties of the brain according to anatomy in healthy controls, reporting that white matter is generally stiffer than cortical gray matter but less stiff than subcortical gray matter [26,65-67]. Others examined the effect of age, and found a gradual decrease in brain stiffness with age [13,31,68,69] (Fig. 8). In addition, some recent studies have reported that brain MRE can depict the association of the mechanical properties of brain tissue with functional processes, such as cognitive function, language function, vascular conditions, and visual stimuli [70-75].

Several brain MRE studies have reported that tumor stiffness assessed using MRE correlates with manual palpation findings in intracranial tumors [76-78]. In addition, relationships between tumor stiffness and tumor entity, glioma grade, and isocitrate dehydrogenase 1 mutation status have been reported [79,80]. Moreover, brain MRE can predict adhesions between brain tissue and extra-axial tumors [81,82].

Brain MRE has been applied in various neurodegenerative diseases to assess its potential as a biomarker. Several studies have found decreased stiffness in the global brain, hippocampus, and cortical gray matter in patients with Alzheimer's disease (AD) [22,83,84]. ElSheikh et al. [85] demonstrated that the four most common causes of dementia (AD, dementia with Lewy bodies, frontotemporal dementia, and normal pressure hydrocephalus) show distinct stiffness patterns, indicating that MRE may serve as a differentiating biomarker. In addition, a decrease in brain stiffness with variations in specific regions was observed in both

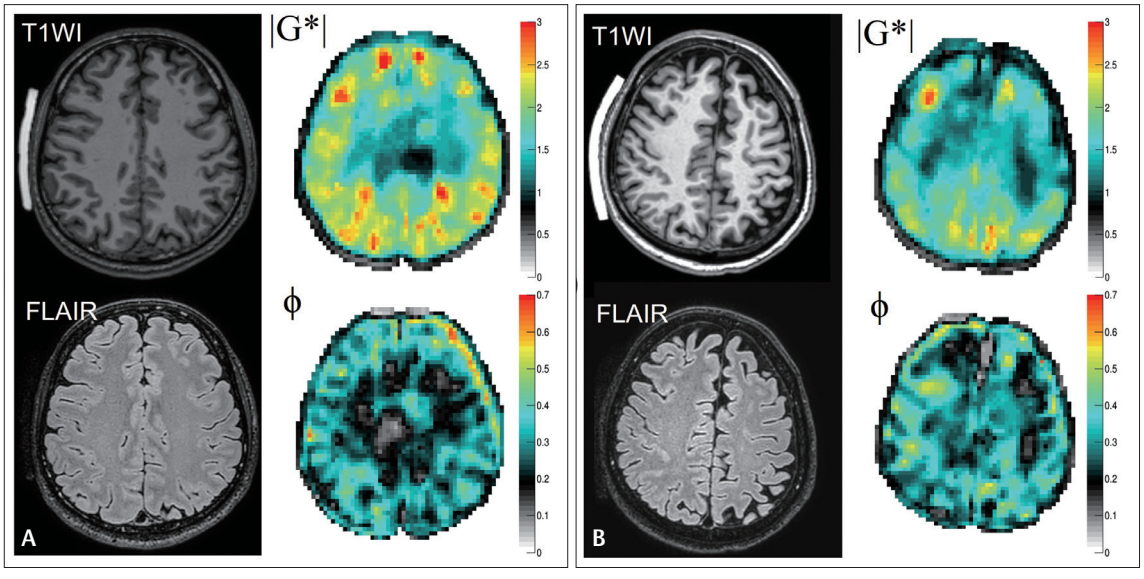

Fig. 8. Examples of brain MRE of a 34-year-old male (A) and a 70-year-old male (B). The younger participant in (A) showed a higher magnitude of the complex shear modulus (|*G**|) than the older participant in (B). Adapted from Joo et al. [31], Korean J Radiol 2023;24:564-573, under CC BY NC license. MRE, magnetic resonance elastography; T1WI, T1-weighted imaging; FLAIR, fluid-attenuated inversion recovery imaging; φ, phase angle of the complex shear modulus.

Parkinson's disease and progressive supranuclear palsy, suggesting the potential of MRE in differentiating between these two neurodegenerative movement disorders [86]. These studies of neurodegenerative diseases and normal aging emphasize that neurodegenerative changes causing a decrease in brain stiffness, often manifesting as unique patterns.

Others

MRE is a promising method for the biomechanical analysis of skeletal muscles that can identify neuromuscular diseases and evaluate the efficacy of treatments. Additionally, it has been reported to be effective in detecting and quantifying changes in muscle stiffness related to normal aging, which may be valuable in assessing sarcopenia [87-94].

MRE has been investigated in the prostate, focusing on its capability for the detection and precise spatial localization of prostate cancer. Notably, diverse driver system techniques have been explored in prostate MRE to optimize the balance between high-frequency shear wave attenuation and the limited spatial resolution encountered with long wavelengths, such as external drivers attached to the pubic bone, transurethral actuators, endorectal actuators, and transperineal driver [95-100].

In addition, MRE has been applied to a range of organs, mainly focusing on evaluating technical feasibility and conducting preliminary pilot studies, including the breast [101-105], heart [106-109], aorta [110-112], lung [113-115], pancreas [116-118], intervertebral disc [119-121], head and neck [122,123], bowel [124], and mesenteric adipose tissue [125]. Although MRE of these organs is currently in the investigational phase, these studies pave the way for future in-depth research, and may contribute to an improved understanding of disease processes.

Limitations, Recent Advancements, and Future Perspectives

The main obstacle to the clinical application of MRE is the absence of standardized methodologies and terminology, particularly for organs other than the liver. Recently, researchers have established guidelines for MRE and standardized the terminology and practices [2]. Using this approach, MRE can provide normative and reliable values, allowing for more extensive clinical investigations.

Another issue is the validation of the MRE results. The accuracy of shear modulus measurements from MRE has been questioned because of the lack of established methods for producing phantoms with precise mechanical properties matching those of biological tissues. Therefore, most validations of quantitative biomarkers obtained with MRE have been based on measurements of precision, that is, by comparing repeated measurements [2].

The assumption of local homogeneity may yield inaccurate estimates near boundaries. This issue becomes pronounced when placing a ROI. Hence, it is recommended to erode the ROI away from the edges of the target structures to reduce the impact of boundary artifacts [2]. Meanwhile, the assumption of isotropy is evidently incorrect in certain soft tissues, such as muscle and white matter fibers. Several studies have proposed inversion algorithms for these materials that utilize information from diffusion tensor imaging [126,127].

The wavelength to pixel ratio significantly affects the accuracy of MRE measurements; the measurement error increases when there are fewer pixels per wavelength, whereas the signal-to-noise ratio decreases when more pixels are obtained by decreasing their size [2,128,129]. This phenomenon may be more pronounced in certain organs, such as the brain, where complex wave fields are prominently generated [130]. Recent studies have addressed this issue [129,131].

Beyond applying external vibration sources, few studies have utilized cardiac pulsation as the vibration source, which is termed intrinsic activation [132,133]. In addition, a diffusion-weighted imaging-based virtual elastography was recently proposed [134-136]. Although their accuracy and reliability require validation, these methods may offer potential alternatives to MRE without necessitating the application of external mechanical vibrations.

CONCLUSION

MRE is a powerful tool that provides information on the mechanical properties of soft tissue, which is beyond the scope of conventional morphological imaging modalities. While the existing body of research on MRE is focusing on CLD, its potential applications in other organs are continuously expanding, promising a deeper understanding of various disease processes. Furthermore, as efforts are made to standardize MRE terminology and protocols, more extensive clinical investigations using MRE are expected in the future.

Conflicts of Interest

The authors have no potential conflicts of interest to disclose.

Author Contributions

Conceptualization: Bio Joo. Data curation: Mina Park, Sung Jun Ahn, Sang Hyun Suh. Formal analysis: Bio Joo. Investigation: Seungtae Lee, Bio Joo. Methodology: Bio Joo. Resources: Bio Joo, Mina Park, Sung Jun Ahn, Sang Hyun Suh. Supervision: Sang Hyun Suh. Validation: Bio Joo. Visualization: Bio Joo. Writing—original draft: Seungtae Lee. Writing—review & editing: Seungtae Lee, Bio Joo, Mina Park, Sung Jun Ahn.

ORCID iDs

Seungtae Lee https://orcid.org/0009-0001-8320-0838
Bio Joo https://orcid.org/0000-0001-7460-1421
Mina Park https://orcid.org/0000-0002-2005-7560
Sung Jun Ahn https://orcid.org/0000-0003-0075-2432
Sang Hyun Suh https://orcid.org/0000-0002-7098-4901

Funding Statement

None

Acknowledgments

We appreciate the Medical Illustration & Design (MID) team, a member of Medical Research Support Services of Yonsei University College of Medicine, for their excellent support with medical illustration.

REFERENCES

1. Muthupillai R, Lomas DJ, Rossman PJ, Greenleaf JF, Manduca A, Ehman RL. Magnetic resonance elastography by direct visualization of propagating acoustic strain waves. Science 1995;269:1854-1857.
2. Manduca A, Bayly PJ, Ehman RL, et al. MR elastography: principles, guidelines, and terminology. Magn Reson Med 2021;85:2377-2390.
3. Chalasani N, Younossi Z, Lavine JE, et al. The diagnosis and management of nonalcoholic fatty liver disease: practice guidance from the American Association for the Study of Liver Diseases. Hepatology 2018;67:328-357.
4. Low G, Kruse SA, Lomas DJ. General review of magnetic resonance elastography. World J Radiol 2016;8:59-72.
5. Hiscox LV, Johnson CL, Barnhill E, et al. Magnetic resonance elastography (MRE) of the human brain: technique, findings and clinical applications. Phys Med Biol 2016;61:R401-R437.
6. Hirsch S, Braun J, Sack I. Magnetic resonance elastography: physical background and medical applications. Weinheim: WILEY-VCH, 2016.
7. Burlew MM, Madsen EL, Zagzebski JA, Banjavic RA, Sum SW. A new ultrasound tissue-equivalent material. Radiology 1980;134:517-520.
8. Manduca A, Oliphant TE, Dresner MA, et al. Magnetic resonance elastography: non-invasive mapping of tissue elasticity. Med Image Anal 2001;5:237-254.
9. Johnson CL, Schwarb H, D J McGarry M, et al. Viscoelasticity of subcortical gray matter structures. Hum Brain Mapp 2016;37:4221-4233.
10. Riek K, Millward JM, Hamann I, et al. Magnetic resonance elastography reveals altered brain viscoelasticity in experimental autoimmune encephalomyelitis. Neuroimage Clin 2012;1:81-90.
11. Li Y, Gao Q, Chen N, et al. Clinical studies of magnetic resonance elastography from 1995 to 2021: scientometric and visualization analysis based on CiteSpace. Quant Imaging Med Surg 2022;12:5080-5100.
12. Klatt D, Hamhaber U, Asbach P, Braun J, Sack I. Noninvasive assessment of the rheological behavior of human organs using multifrequency MR elastography: a study of brain and liver viscoelasticity. Phys Med Biol 2007;52:7281-7294.
13. Sack I, Beierbach B, Wuerfel J, et al. The impact of aging and gender on brain viscoelasticity. Neuroimage 2009;46:652-657.
14. Sack I, Jöhrens K, Würfel J, Braun J. Structure-sensitive elastography: on the viscoelastic powerlaw behavior of in vivo human tissue in health and disease. Soft matter 2013;9:5672-5680.
15. Asbach P, Klatt D, Hamhaber U, et al. Assessment of liver viscoelasticity using multifrequency MR elastography. Magn Reson Med 2008;60:373-379.
16. Guo J, Posnansky O, Hirsch S, et al. Fractal network dimension and viscoelastic powerlaw behavior: II. an experimental study of structure-mimicking phantoms by magnetic resonance elastography. Phys Med Biol 2012;57:4041-4053.
17. Urayama K, Kawamura T, Kohjiya SJP. Structure–mechanical property correlations of model siloxane elastomers with controlled network topology. Polymer 2009;50:347-356.
18. Baumgart E. Stiffness--an unknown world of mechanical science? Injury 2000;31 Suppl 2:S-B14-23.
19. Allen AM, Shah VH, Therneau TM, et al. the role of three-dimensional magnetic resonance elastography in the diagnosis of nonalcoholic steatohepatitis in obese patients undergoing bariatric surgery. Hepatology 2020;71:510-521.
20. Yin M, Talwalkar JA, Glaser KJ, et al. Assessment of hepatic fibrosis with magnetic resonance elastography. Clin Gastroenterol Hepatol 2007;5:1207-1213.e2.
21. Glaser KJ, Manduca A, Ehman RL. Review of MR elastography applications and recent developments. J Magn Reson Imaging 2012;36:757-774.
22. Murphy MC, Huston J 3rd, Jack CR Jr, et al. Decreased brain stiffness in Alzheimer's disease determined by magnetic resonance elastography. J Magn Reson Imaging 2011;34:494-498.
23. Huston J 3rd, Murphy MC, Boeve BF, et al. Magnetic resonance elastography of frontotemporal dementia. J Magn Reson Imaging 2016;43:474-478.
24. Venkatesh SK, Yin M, Ehman RL. Magnetic resonance elastography of liver: technique, analysis, and clinical applications. J Magn Reson Imaging 2013;37:544-555.
25. Johnson CL, McGarry MD, Van Houten EE, et al. Magnetic resonance elastography of the brain using multishot spiral readouts with self-navigated motion correction. Magn Reson Med 2013;70:404-412.
26. Braun J, Guo J, Lützkendorf R, et al. High-resolution mechanical imaging of the human brain by three-dimensional multifrequency magnetic resonance elastography at 7T. Neuroimage 2014;90:308-314.
27. Uffmann K, Ladd ME. Actuation systems for MR elastography: design and applications. IEEE Eng Med Biol Mag 2008;27:28-34.
28. Guo J, Hirsch S, Fehlner A, et al. Towards an elastographic atlas of brain anatomy. PLoS One 2013;8:e71807.
29. Runge JH, Hoelzl SH, Sudakova J, et al. A novel magnetic resonance elastography transducer concept based on a rotational eccentric mass: preliminary experiences with the gravitational

transducer. Phys Med Biol 2019;64:045007.
30. Svensson SF, De Arcos J, Darwish OI, et al. Robustness of mr elastography in the healthy brain: repeatability, reliability, and effect of different reconstruction methods. J Magn Reson Imaging 2021;53:1510-1521.
31. Joo B, Won SY, Sinkus R, Lee SK. Viscoelastic property of the brain assessed with magnetic resonance elastography and its association with glymphatic system in neurologically normal individuals. Korean J Radiol 2023;24:564-573.
32. Sinkus R, Lorenzen J, Schrader D, Lorenzen M, Dargatz M, Holz D. High-resolution tensor MR elastography for breast tumour detection. Phys Med Biol 2000;45:1649-1664.
33. Manduca A, Rossman TL, Lake DS, et al. Waveguide effects and implications for cardiac magnetic resonance elastography: a finite element study. NMR Biomed 2018 Aug 13. [Epub]. https://doi.org/10.1002/nbm.3996.
34. Baghani A, Salcudean S, Rohling R. Theoretical limitations of the elastic wave equation inversion for tissue elastography. J Acoust Soc Am 2009;126:1541.
35. Shi Y, Qi YF, Lan GY, et al. Three-dimensional MR elastography depicts liver inflammation, fibrosis, and portal hypertension in chronic hepatitis B or C. Radiology 2021;301:154-162.
36. Johnson CL, Holtrop JL, McGarry MD, et al. 3D multislab, multishot acquisition for fast, whole-brain MR elastography with high signal-to-noise efficiency. Magn Reson Med 2014;71:477-485.
37. Fovargue D, Nordsletten D, Sinkus R. Stiffness reconstruction methods for MR elastography. NMR Biomed 2018;31:e3935.
38. Oliphant TE, Manduca A, Ehman RL, Greenleaf JF. Complex-valued stiffness reconstruction for magnetic resonance elastography by algebraic inversion of the differential equation. Magn Reson Med 2001;45:299-310.
39. McGarry MD, Van Houten EE, Johnson CL, et al. Multiresolution MR elastography using nonlinear inversion. Med Phys 2012;39:6388-6396.
40. Fovargue D, Kozerke S, Sinkus R, Nordsletten D. Robust MR elastography stiffness quantification using a localized divergence free finite element reconstruction. Med Image Anal 2018;44:126-142.
41. Honarvar M, Rohling R, Salcudean SE. A comparison of direct and iterative finite element inversion techniques in dynamic elastography. Phys Med Biol 2016;61:3026-3048.
42. Honarvar M, Sahebjavaher R, Sinkus R, Rohling R, Salcudean SE. Curl-based finite element reconstruction of the shear modulus without assuming local homogeneity: time harmonic case. IEEE Trans Med Imaging 2013;32:2189-2199.
43. Asbach P, Klatt D, Schlosser B, et al. Viscoelasticity-based staging of hepatic fibrosis with multifrequency MR elastography. Radiology 2010;257:80-86.
44. Hirsch S, Guo J, Reiter R, et al. MR elastography of the liver and the spleen using a piezoelectric driver, single-shot wave-field acquisition, and multifrequency dual parameter reconstruction. Magn Reson Med 2014;71:267-277.
45. Fehlner A, Behrens JR, Streitberger KJ, et al. Higher-resolution MR elastography reveals early mechanical signatures of neuroinflammation in patients with clinically isolated syndrome. J Magn Reson Imaging 2016;44:51-58.
46. Serai SD, Obuchowski NA, Venkatesh SK, et al. Repeatability of MR elastography of liver: a meta-analysis. Radiology 2017;285:92-100.
47. Venkatesh SK, Wang G, Teo LL, Ang BW. Magnetic resonance elastography of liver in healthy Asians: normal liver stiffness quantification and reproducibility assessment. J Magn Reson Imaging 2014;39:1-8.
48. Cui J, Heba E, Hernandez C, et al. Magnetic resonance elastography is superior to acoustic radiation force impulse for the Diagnosis of fibrosis in patients with biopsy-proven nonalcoholic fatty liver disease: a prospective study. Hepatology 2016;63:453-461.
49. Singh S, Venkatesh SK, Loomba R, et al. Magnetic resonance elastography for staging liver fibrosis in non-alcoholic fatty liver disease: a diagnostic accuracy systematic review and individual participant data pooled analysis. Eur Radiol 2016;26:1431-1440.
50. Trout AT, Serai S, Mahley AD, et al. Liver stiffness measurements with MR elastography: agreement and repeatability across imaging systems, field strengths, and pulse sequences. Radiology 2016;281:793-804.
51. Guglielmo FF, Venkatesh SK, Mitchell DG. Liver MR elastography technique and image interpretation: pearls and pitfalls. Radiographics 2019;39:1983-2002.
52. Idilman IS, Li J, Yin M, Venkatesh SK. MR elastography of liver: current status and future perspectives. Abdom Radiol (NY) 2020;45:3444-3462.
53. Expert Panel on Gastrointestinal Imaging; Bashir MR, Horowitz JM, et al. ACR Appropriateness Criteria(R) chronic liver disease. J Am Coll Radiol 2020;17(5S):S70-S80.
54. Singh S, Venkatesh SK, Wang Z, et al. Diagnostic performance of magnetic resonance elastography in staging liver fibrosis: a systematic review and meta-analysis of individual participant data. Clin Gastroenterol Hepatol 2015;13:440-451.e6.
55. Su LN, Guo SL, Li BX, Yang P. Diagnostic value of magnetic resonance elastography for detecting and staging of hepatic fibrosis: a meta-analysis. Clin Radiol 2014;69:e545-e552.
56. Motosugi U, Ichikawa T, Koshiishi T, et al. Liver stiffness measured by magnetic resonance elastography as a risk factor for hepatocellular carcinoma: a preliminary case-control study. Eur Radiol 2013;23:156-162.
57. Lee DH, Lee JM, Chang W, et al. Prognostic role of liver stiffness measurements using magnetic resonance elastography in patients with compensated chronic liver disease. Eur Radiol 2018;28:3513-3521.
58. Ichikawa S, Motosugi U, Enomoto N, Onishi H. Magnetic resonance elastography can predict development of hepatocellular carcinoma with longitudinally acquired two-point data. Eur Radiol 2019;29:1013-1021.
59. Sun HY, Lee JM, Han JK, Choi BI. Usefulness of MR elastography for predicting esophageal varices in cirrhotic patients. J Magn Reson Imaging 2014;39:559-566.
60. Abe H, Midorikawa Y, Matsumoto N, et al. Prediction of esoph-

ageal varices by liver and spleen MR elastography. Eur Radiol 2019;29:6611-6619.
61. Ronot M, Lambert S, Elkrief L, et al. Assessment of portal hypertension and high-risk oesophageal varices with liver and spleen three-dimensional multifrequency MR elastography in liver cirrhosis. Eur Radiol 2014;24:1394-1402.
62. Asrani SK, Talwalkar JA, Kamath PS, et al. Role of magnetic resonance elastography in compensated and decompensated liver disease. J Hepatol 2014;60:934-939.
63. Sack I, Beierbach B, Hamhaber U, Klatt D, Braun J. Non-invasive measurement of brain viscoelasticity using magnetic resonance elastography. NMR Biomed 2008;21:265-271.
64. Arani A, Manduca A, Ehman RL, Huston Iii J. Harnessing brain waves: a review of brain magnetic resonance elastography for clinicians and scientists entering the field. Br J Radiol 2021;94: 20200265.
65. Johnson CL, McGarry MD, Gharibans AA, et al. Local mechanical properties of white matter structures in the human brain. Neuroimage 2013;79:145-152.
66. Zhang J, Green MA, Sinkus R, Bilston LE. Viscoelastic properties of human cerebellum using magnetic resonance elastography. J Biomech 2011;44:1909-1913.
67. Hiscox LV, McGarry MDJ, Schwarb H, et al. Standard-space atlas of the viscoelastic properties of the human brain. Hum Brain Mapp 2020;41:5282-5300.
68. Arani A, Murphy MC, Glaser KJ, et al. Measuring the effects of aging and sex on regional brain stiffness with MR elastography in healthy older adults. Neuroimage 2015;111:59-64.
69. Hiscox LV, Johnson CL, McGarry MDJ, et al. High-resolution magnetic resonance elastography reveals differences in subcortical gray matter viscoelasticity between young and healthy older adults. Neurobiol Aging 2018;65:158-167.
70. Schwarb H, Johnson CL, McGarry MDJ, Cohen NJ. Medial temporal lobe viscoelasticity and relational memory performance. Neuroimage 2016;132:534-541.
71. Schwarb H, Johnson CL, Daugherty AM, et al. Aerobic fitness, hippocampal viscoelasticity, and relational memory performance. Neuroimage 2017;153:179-188.
72. Sandroff BM, Johnson CL, Motl RW. Exercise training effects on memory and hippocampal viscoelasticity in multiple sclerosis: a novel application of magnetic resonance elastography. Neuroradiology 2017;59:61-67.
73. Schneider JM, McIlvain G, Johnson CL. Mechanical properties of the developing brain are associated with language input and vocabulary outcome. Dev Neuropsychol 2022;47:258-272.
74. Sanjana F, Delgorio PL, DeConne TM, et al. Vascular determinants of hippocampal viscoelastic properties in healthy adults across the lifespan. J Cereb Blood Flow Metab 2023;43:1931-1941.
75. Lan PS, Glaser KJ, Ehman RL, Glover GH. Imaging brain function with simultaneous BOLD and viscoelasticity contrast: fMRI/fMRE. Neuroimage 2020;211:116592.
76. Murphy MC, Huston J 3rd, Glaser KJ, et al. Preoperative assessment of meningioma stiffness using magnetic resonance elastography. J Neurosurg 2013;118:643-648.
77. Sakai N, Takehara Y, Yamashita S, et al. Shear stiffness of 4 common intracranial tumors measured using MR elastography: comparison with intraoperative consistency grading. AJNR Am J Neuroradiol 2016;37:1851-1859.
78. Hughes JD, Fattahi N, Van Gompel J, et al. Higher-resolution magnetic resonance elastography in meningiomas to determine intratumoral consistency. Neurosurgery 2015;77:653-658;discussion 658-659.
79. Pepin KM, McGee KP, Arani A, et al. MR elastography analysis of glioma stiffness and IDH1-mutation status. AJNR Am J Neuroradiol 2018;39:31-36.
80. Reiss-Zimmermann M, Streitberger KJ, Sack I, et al. High resolution imaging of viscoelastic properties of intracranial tumours by multi-frequency magnetic resonance elastography. Clin Neuroradiol 2015;25:371-378.
81. Yin Z, Glaser KJ, Manduca A, et al. Slip interface imaging predicts tumor-brain adhesion in vestibular schwannomas. Radiology 2015;277:507-517.
82. Yin Z, Hughes JD, Trzasko JD, et al. Slip interface imaging based on MR-elastography preoperatively predicts meningioma-brain adhesion. J Magn Reson Imaging 2017;46:1007-1016.
83. Gerischer LM, Fehlner A, Köbe T, et al. Combining viscoelasticity, diffusivity and volume of the hippocampus for the diagnosis of Alzheimer's disease based on magnetic resonance imaging. Neuroimage Clin 2017;18:485-493.
84. Hiscox LV, Johnson CL, McGarry MDJ, et al. Mechanical property alterations across the cerebral cortex due to Alzheimer's disease. Brain Commun 2020;2:fcz049.
85. ElSheikh M, Arani A, Perry A, et al. MR elastography demonstrates unique regional brain stiffness patterns in dementias. AJR Am J Roentgenol 2017;209:403-408.
86. Lipp A, Skowronek C, Fehlner A, Streitberger KJ, Braun J, Sack I. Progressive supranuclear palsy and idiopathic Parkinson's disease are associated with local reduction of in vivo brain viscoelasticity. Eur Radiol 2018;28:3347-3354.
87. Ringleb SI, Bensamoun SF, Chen Q, Manduca A, An KN, Ehman RL. Applications of magnetic resonance elastography to healthy and pathologic skeletal muscle. J Magn Reson Imaging 2007; 25:301-309.
88. Domire ZJ, McCullough MB, Chen Q, An KN. Feasibility of using magnetic resonance elastography to study the effect of aging on shear modulus of skeletal muscle. J Appl Biomech 2009;25: 93-97.
89. McCullough MB, Domire ZJ, Reed AM, et al. Evaluation of muscles affected by myositis using magnetic resonance elastography. Muscle Nerve 2011;43:585-590.
90. Basford JR, Jenkyn TR, An KN, Ehman RL, Heers G, Kaufman KR. Evaluation of healthy and diseased muscle with magnetic resonance elastography. Arch Phys Med Rehabil 2002;83:1530-1536.
91. Hong SH, Hong SJ, Yoon JS, et al. Magnetic resonance elastography (MRE) for measurement of muscle stiffness of the shoulder: feasibility with a 3 T MRI system. Acta Radiol 2016;57:1099-1106.

92. Ito D, Numano T, Ueki T, et al. Magnetic resonance elastography of the supraspinatus muscle: a preliminary study on test-retest repeatability and wave quality with different frequencies and image filtering. Magn Reson Imaging 2020;71:27-36.
93. Bensamoun SF, Ringleb SI, Littrell L, et al. Determination of thigh muscle stiffness using magnetic resonance elastography. J Magn Reson Imaging 2006;23:242-247.
94. Chakouch MK, Charleux F, Bensamoun SF. Quantifying the elastic property of nine thigh muscles using magnetic resonance elastography. PLoS One 2015;10:e0138873.
95. Arani A, Plewes D, Krieger A, Chopra R. The feasibility of endorectal MR elastography for prostate cancer localization. Magn Reson Med 2011;66:1649-1657.
96. Sahebjavaher RS, Baghani A, Honarvar M, Sinkus R, Salcudean SE. Transperineal prostate MR elastography: initial in vivo results. Magn Reson Med 2013;69:411-420.
97. Li S, Chen M, Wang W, et al. A feasibility study of MR elastography in the diagnosis of prostate cancer at 3.0T. Acta Radiol 2011; 52:354-358.
98. Deng Y, Yi Z, Zhang T, et al. Magnetic resonance elastography of the prostate in patients with lower urinary tract symptoms: feasibility of the modified driver at high multi-frequencies. Abdom Radiol (NY) 2022;47:399-408.
99. Asbach P, Ro SR, Aldoj N, et al. In vivo quantification of water diffusion, stiffness, and tissue fluidity in benign prostatic hyperplasia and prostate cancer. Invest Radiol 2020;55:524-530.
100. Kemper J, Sinkus R, Lorenzen J, Nolte-Ernsting C, Stork A, Adam G. MR elastography of the prostate: initial in-vivo application. Rofo 2004;176:1094-1099.
101. McKnight AL, Kugel JL, Rossman PJ, Manduca A, Hartmann LC, Ehman RL. MR elastography of breast cancer: preliminary results. AJR Am J Roentgenol 2002;178:1411-1417.
102. Sinkus R, Tanter M, Xydeas T, Catheline S, Bercoff J, Fink M. Viscoelastic shear properties of in vivo breast lesions measured by MR elastography. Magn Reson Imaging 2005;23:159-165.
103. Siegmann KC, Xydeas T, Sinkus R, Kraemer B, Vogel U, Claussen CD. Diagnostic value of MR elastography in addition to contrast-enhanced MR imaging of the breast-initial clinical results. Eur Radiol 2010;20:318-325.
104. Sinkus R, Siegmann K, Xydeas T, Tanter M, Claussen C, Fink M. MR elastography of breast lesions: understanding the solid/liquid duality can improve the specificity of contrast-enhanced MR mammography. Magn Reson Med 2007;58:1135-1144.
105. Hawley JR, Kalra P, Mo X, Raterman B, Yee LD, Kolipaka A. Quantification of breast stiffness using MR elastography at 3 Tesla with a soft sternal driver: a reproducibility study. J Magn Reson Imaging 2017;45:1379-1384.
106. Kolipaka A, McGee KP, Manduca A, Anavekar N, Ehman RL, Araoz PA. In vivo assessment of MR elastography-derived effective end-diastolic myocardial stiffness under different loading conditions. J Magn Reson Imaging 2011;33:1224-1228.
107. Elgeti T, Beling M, Hamm B, Braun J, Sack I. Cardiac magnetic resonance elastography: toward the diagnosis of abnormal myocardial relaxation. Invest Radiol 2010;45:782-787.
108. Sui Y, Arunachalam SP, Arani A, et al. Cardiac MR elastography using reduced-FOV, single-shot, spin-echo EPI. Magn Reson Med 2018;80:231-238.
109. Arani A, Arunachalam SP, Chang ICY, et al. Cardiac MR elastography for quantitative assessment of elevated myocardial stiffness in cardiac amyloidosis. J Magn Reson Imaging 2017;46:1361-1367.
110. Damughatla AR, Raterman B, Sharkey-Toppen T, et al. Quantification of aortic stiffness using MR elastography and its comparison to MRI-based pulse wave velocity. J Magn Reson Imaging 2015;41:44-51.
111. Kenyhercz WE, Raterman B, Illapani VS, et al. Quantification of aortic stiffness using magnetic resonance elastography: Measurement reproducibility, pulse wave velocity comparison, changes over cardiac cycle, and relationship with age. Magn Reson Med 2016;75:1920-1926.
112. Dong H, Jin N, Kannengiesser S, Raterman B, White RD, Kolipaka A. Magnetic resonance elastography for estimating in vivo stiffness of the abdominal aorta using cardiac-gated spin-echo echo-planar imaging: a feasibility study. NMR Biomed 2021;34:e4420.
113. Fakhouri F, Kannengiesser S, Pfeuffer J, Gokun Y, Kolipaka A. Free-breathing MR elastography of the lungs: an in vivo study. Magn Reson Med 2022;87:236-248.
114. Fakhouri F, Dong H, Kolipaka A. Magnetic resonance elastography of the lungs: a repeatability and reproducibility study. NMR Biomed 2019;32:e4102.
115. Marinelli JP, Levin DL, Vassallo R, et al. Quantitative assessment of lung stiffness in patients with interstitial lung disease using MR elastography. J Magn Reson Imaging 2017;46:365-374.
116. Shi Y, Glaser KJ, Venkatesh SK, Ben-Abraham EI, Ehman RL. Feasibility of using 3D MR elastography to determine pancreatic stiffness in healthy volunteers. J Magn Reson Imaging 2015;41: 369-375.
117. Kolipaka A, Schroeder S, Mo X, Shah Z, Hart PA, Conwell DL. Magnetic resonance elastography of the pancreas: measurement reproducibility and relationship with age. Magn Reson Imaging 2017;42:1-7.
118. Liu D, Chen J, Zhang Y, Dai Y, Yao X. Magnetic resonance elastography-derived stiffness: potential imaging biomarker for differentiation of benign and malignant pancreatic masses. Abdom Radiol (NY) 2023;48:2604-2614.
119. Co M, Dong H, Boulter DJ, et al. Magnetic resonance elastography of intervertebral discs: spin-echo echo-planar imaging sequence validation. J Magn Reson Imaging 2022;56:1722-1732.
120. Walter BA, Mageswaran P, Mo X, et al. MR elastography-derived stiffness: a biomarker for intervertebral disc degeneration. Radiology 2017;285:167-175.
121. Ben-Abraham EI, Chen J, Felmlee JP, et al. Feasibility of MR elastography of the intervertebral disc. Magn Reson Imaging 2017; 39:132-137.
122. Yeung DK, Bhatia KS, Lee YY, et al. MR elastography of the head and neck: driver design and initial results. Magn Reson Imaging 2013;31:624-629.
123. Elsholtz FHJ, Reiter R, Marticorena Garcia SR, et al. Multifre-

quency magnetic resonance elastography-based tomoelastography of the parotid glands-feasibility and reference values. Dentomaxillofac Radiol 2022;51:20210337.
124. Reiter R, Loch FN, Kamphues C, et al. Feasibility of intestinal MR elastography in inflammatory bowel disease. J Magn Reson Imaging 2022;55:815-822.
125. Jensen LJ, Loch FN, Kamphues C, et al. Feasibility of in vivo magnetic resonance elastography of mesenteric adipose tissue in Crohn's disease. Quant Imaging Med Surg 2023;13:4792-4805.
126. Romano A, Scheel M, Hirsch S, Braun J, Sack I. In vivo waveguide elastography of white matter tracts in the human brain. Magn Reson Med 2012;68:1410-1422.
127. Green MA, Geng G, Qin E, Sinkus R, Gandevia SC, Bilston LE. Measuring anisotropic muscle stiffness properties using elastography. NMR Biomed 2013;26:1387-1394.
128. Hu L. Requirements for accurate estimation of shear modulus by magnetic resonance elastography: a computational comparative study. Comput Methods Programs Biomed 2020;192:105437.
129. Mura J, Schrank F, Sack I. An analytical solution to the dispersion-by-inversion problem in magnetic resonance elastography. Magn Reson Med 2020;84:61-71.
130. Clayton EH, Genin GM, Bayly PV. Transmission, attenuation and reflection of shear waves in the human brain. J R Soc Interface 2012;9:2899-2910.
131. Kabir IE, Caban-Rivera DA, Ormachea J, Parker KJ, Johnson CL, Doyley MM. Reverberant magnetic resonance elastographic imaging using a single mechanical driver. Phys Med Biol 2023;68:055015.
132. Weaver JB, Pattison AJ, McGarry MD, et al. Brain mechanical property measurement using MRE with intrinsic activation. Phys Med Biol 2012;57:7275-7287.
133. Solamen LM, McGarry MDJ, Fried J, Weaver JB, Lollis SS, Paulsen KD. Poroelastic mechanical properties of the brain tissue of normal pressure hydrocephalus patients during lumbar drain treatment using intrinsic actuation MR elastography. Acad Radiol 2021;28:457-466.
134. Kromrey ML, Le Bihan D, Ichikawa S, Motosugi U. Diffusion-weighted MRI-based virtual elastography for the assessment of liver fibrosis. Radiology 2020;295:127-135.
135. Le Bihan D, Ichikawa S, Motosugi U. Diffusion and intravoxel incoherent motion MR imaging-based virtual elastography: a hypothesis-generating study in the liver. Radiology 2017;285:609-619.
136. Aunan-Diop JS, Andersen MCS, Friismose AI, et al. Virtual magnetic resonance elastography predicts the intraoperative consistency of meningiomas. J Neuroradiol 2023;50:396-401.
137. Klatt D, Johnson CL, Magin RL. Simultaneous, multidirectional acquisition of displacement fields in magnetic resonance elastography of the in vivo human brain. J Magn Reson Imaging 2015;42:297-304.
138. Ringe KI, Yoon JH. Strategies and Techniques for Liver Magnetic Resonance Imaging: New and Pending Applications for Routine Clinical Practice. Korean J Radiol 2023;24:180-189.